Reversible, Band-Gap-Selective Protonation of Single-Walled Carbon Nanotubes in Solution

Michael S. Strano,[†] Chad B. Huffman,[†] Valerie C. Moore,[†] Michael J. O'Connell,[†] Erik H. Haroz,[†] Jarred Hubbard,[†] Michael Miller,[†] Kristy Rialon,[†] Carter Kittrell,[†] Sivarajan Ramesh,[†] Robert H. Hauge,[†] and Richard E. Smalley*[,†,‡]

Department of Chemistry, Center for Nanoscale Science and Technology, and Center for Biological and Environmental Nanotechnology, and Department of Physics, Rice University, 6100 Main Street, Houston, Texas 77005

Received: December 9, 2002; In Final Form: April 15, 2003

In acidic solution between pH 6 and 2.5, protons react reversibly and selectively in the presence of preadsorbed oxygen at the sidewall of aqueous dispersed single-walled carbon nanotubes suspended in sodium dodecyl sulfate. This reactive complex, which protonates the nanotube sidewall, reversibly diminishes absorption intensity, fluorescent emission, and resonant Raman scattering intensity. The results document the first evidence of electronic selectivity with metallic nanotubes reacting initially near neutral pH, followed by successive protonation of nanotubes with increasing band gap as the solution is increasingly acidified. Preadsorption of molecular oxygen is shown to play a critical role in the interaction, and its desorption kinetics is followed using UV irradiation. The role of the charged electric double layer of the surfactant is discussed. This chemistry, which proceeds under relatively mild conditions, holds promise for separating nanotubes by metal and semiconducting types.

Introduction

Single-walled fullerene nanotubes[1] are currently the focus of intense research activity because of their unique physical and chemical properties and their prospects for novel technologies.[2] While these properties are diverse, varying with nanotube chirality and diameter, attempts to utilize and explore their unique chemistry in solution have been complicated by sample aggregation and hence the inability to differentiate between distinctly metallic and semiconducting nanotubes. Nanotubes readily form aggregates of aligned tubes in bundles or "ropes" with a sizable tube−tube binding energy of 500 eV/μm.[3,4] These aggregates generally contain random mixtures of metallic and semiconducting types as well as assorted nanotube diameters. When in electrical contact in this manner, carbon nanotubes experience sizable perturbations from their otherwise pristine electronic structure.[5]

Hence, the majority of attempts to exploit the chemical diversity within nanotube solutions, either through sidewall functionalization[6] or end group derivitization,[7] for example, have produced largely bundles of nanotubes or nanotubes that otherwise have a significantly altered electronic band structure. The evidence for this has been the relatively unstructured optical absorption spectra,[5] absence of band gap fluorescence,[8] and relative Raman scattering intensities[9,10] in the solution phase commensurate with those of solid nanotube flakes or powders.

Very recent advances in nanotube dispersion provide, for the first time, the ability to monitor the chemical behavior of distinct carbon nanotubes in solution. Band gap fluorescence, a property observed for essentially individually dispersed nanotubes,[8] provides a very sensitive means of probing the electronic structure of semiconducting nanotubes for example. Likewise, once freed from the electronic coupling to their neighbors in aggregates, these well-dispersed nanotubes also show more prominent resonant Raman scatter that is more sensitive to the microenvironment of the nanotube.

This paper provides the first example of the rich and diverse chemical behavior of carbon nanotubes as distinct chemical entities in solution. Specifically, we have found that carbon nanotubes suspended using sodium dodecyl sulfate in water and exposed to ambient O_2 reversibly protonate to form a complex at the nanotube surface that localizes electrons near the Fermi level. This localization diminishes the absorption intensities of the nanotube chromophore, eliminating band gap fluorescence and disrupting the coupling of phonon and electronic states that produce resonance-enhanced Raman scattering. The reaction is completely reversible by adjusting the solution pH to alkaline conditions. We further observe that the reaction is selective to certain chirality and diameter nanotubes. Metallic nanotubes are shown to be the most reactive, protonating near neutral pH, followed by semiconducting nanotubes that increasingly react as the solution is acidified, with the largest band gap nanotubes least reactive.

Experimental Section

Spectrophotometric Titratation. Suspended nanotubes were prepared in a manner reported previously[8] using sodium dodecyl sulfate (99.9%, Sigma-Aldrich) and D_2O (99.9%, Cambridge Isotope Lab.). Titrations were performed in an open, three-necked, 250 mL flask exposed to air with stirring. Raman spectroscopy was performed in-situ using a Kaiser Process Raman spectrometer (Kaiser Optical Inc.) with 20 mW laser intensity focused on the solution in the flask. Excitation wavelengths of 532 and 785 nm were employed. Aliquots of 1 N NaOH or HCl (Fisher Scientific) were added to equilibrate to the desired pH. Equilibration was confirmed by monitoring transient changes in the tangential mode of the Raman spectrum.

* To whom correspondence should be addressed. E-mail: res@rice.edu.
† Department of Chemistry.
‡ Department of Physics.

10.1021/jp027664a CCC: $25.00
Published on Web 06/25/2003

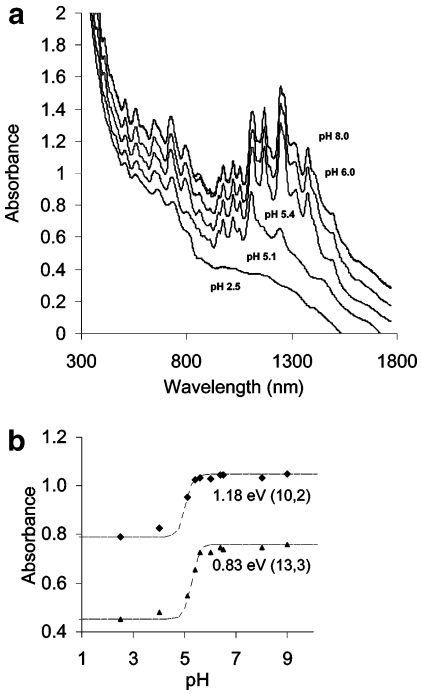

Figure 1. Spectrophotometric titration of individually dispersed carbon nanotubes in SDS suspension. (a) Absorption spectra are offset from pH 8 by a constant value to show changes (pH 6, −0.1; pH 5.4, −0.2; pH 5.1, −0.3; pH 2.5, −0.4). (b) Absorbance plotted as a function of pH for two particular semiconducting nanotubes. The trend is characteristic of an equilibrium-limited surface reaction. Smooth curves represent the regressed model (eq 2) with $n = 3$ and best fit value of K_p for each nanotube.

A 1 mL sample of solution was removed from the flask at each equilibrated pH and the absorbance spectrum was recorded with a Shimadzu UV-3101 Scanning spectrophotometer.

Photodesorption of O_2. The flask was fitted with a sealed 0.5 in. quartz tube that protruded into the liquid. A low-pressure Hg lamp was placed in the center of the tube. The sample was heated to 40 °C for 12 h under N_2 to remove dissolved and some physiorbed oxygen from the sample. Continuous, transient Raman spectroscopy was performed on the solution before and after short intervals of irradiation.

Effect of Other Surfactants. Experiments were repeated using nanotubes analogously suspended[5] in dodecyl trimethylammonium bromide (99% Sigma-Aldrich). Also, additives were coadsorbed in the surfactant layer for SDS-suspended nanotubes under acidic conditions to probe the influence of the Stern layer. Poly(vinylpyrrolidone) (PVP; 40, 360 kDa) and poly(ethylene oxide) (PEO; 70 kDa) were obtained from Sigma-Aldrich and added to solutions equilibrated to pH 2. To examine the effect of polymerization of the hydrophilic additive on the pH dependence, 1-vinyl-2-pyrolydone (Sigma-Aldrich) was used in a similar manner.

Results and Discussion

For semiconducting nanotubes, reaction selectivity is easily followed in the absorption spectrum as a function of solution pH. Reaction at the surface results in the localization of valence electrons that are no longer free to participate in photoabsorption. This substantially diminishes the absorption intensity corresponding to the highest lying valence electrons of the nanotube. In Figure 1a, the solution pH is cycled between 8 and 2.5 and the structured absorption corresponding to the first van Hove or E_{11} transitions, 800−1600 nm, broaden considerably with increasing acidity. The intensities in the second van Hove or E_{22} region from about 550−900 nm arise from electrons with lower energy and are less affected. Smaller optical band gap semiconducting nanotubes, starting at around 1600 nm in Figure 1a, are affected at higher pH than those with larger band gaps. The rates of reaction are also selective. The marked pH dependence and complete reversibility suggest an equilibrium reaction of the nanotube (SWNT) with a number of free protons in solution ($n[H^+]$) resulting in a protonated nanotube complex [P] that has an overall diminished absorption cross section.

$$n[H^+] + \mathrm{SWNT} \overset{K_p}{\longleftrightarrow} [P] \tag{1}$$

Here K_p is the reaction equilibrium constant. Scaling the absorption intensities to yield the fraction of reacted nanotubes and substituting the equilibrium relation above yield:

$$\frac{A(\mathrm{pH}) - A_p}{A_d - A_p} = \frac{K_p}{[H^+]^n + K_p} = \frac{K_p}{10^{-(n\mathrm{pH})} + K_p} \tag{2}$$

In Figure 1b the absorbance for two different band gap semiconducting nanotubes is plotted as a function of pH, and values for n and K_p were regressed using this equilibrium-limited protonation model with A_p and A_d as the absorption intensities of the protonated and deprotoanted states and K_p as the equilibrium constant. Values for $\ln(K_p)$ range from −36.39 for the (12,5) nanotube (0.83 eV band gap) to −33.97 for the (8,3) tube (1.3 eV band gap) The steepness of the curve in Figure 1b is a measure of n or the average number of protons reacting per protonated entity and was determined to be 3. Assignment of optical band gap energies with the (n,m) chirality index was possible using recently successes in nanotube spectroscopy.[11]

Conversely, the electrons near the Fermi energy for metallic nanotubes are difficult to monitor by spectroscopic means, because they possess a broad continuum of electronic states near this point. For all nanotubes, the Raman tangential mode—a line near 1600 cm^{-1} shift arising from the C−C vibrations in sp^2 hybridized systems—splits into high- and low-frequency phonons because the force constants for these bonds are larger in the direction parallel to the tube length than in the orthogonal direction. For metallic nanotubes, the latter is allowed to couple to the continuum of electronic states near the Fermi level, creating a broadened and low-frequency-shifted Breit−Wigner−Fano (BWF) line shape:[12]

$$\frac{I(\omega)}{I_o} = \frac{\left(1 + \frac{(\omega - \omega_o)}{q\Gamma}\right)^2}{1 + \left(\frac{(\omega - \omega_o)}{\Gamma}\right)^2}$$

where Γ, q, and ω_o are broadening, line shape, and frequency renormalization parameters, respectively. Figure 2a shows this low-frequency BWF feature adjacent to a Lorentzian line shape that represents the remaining tangential modes. This region of the spectrum was fit using a composite of both functions. Best-fit values of 42.2 cm^{-1} and 0.20 were obtained for the broadening, Γ, and line shape, $-1/q$, respectively, and were assumed to be constant with respect to pH. As the solution is increasingly acidified and electrons are withdrawn with increasing protonation, this coupling is necessarily disrupted and the BWF line shape predictably shifts to higher frequencies. In Figure 2b it is clear that this feature does not decrease in intensity but rather shifts systematically as the pH is cycled. This is in contrast to

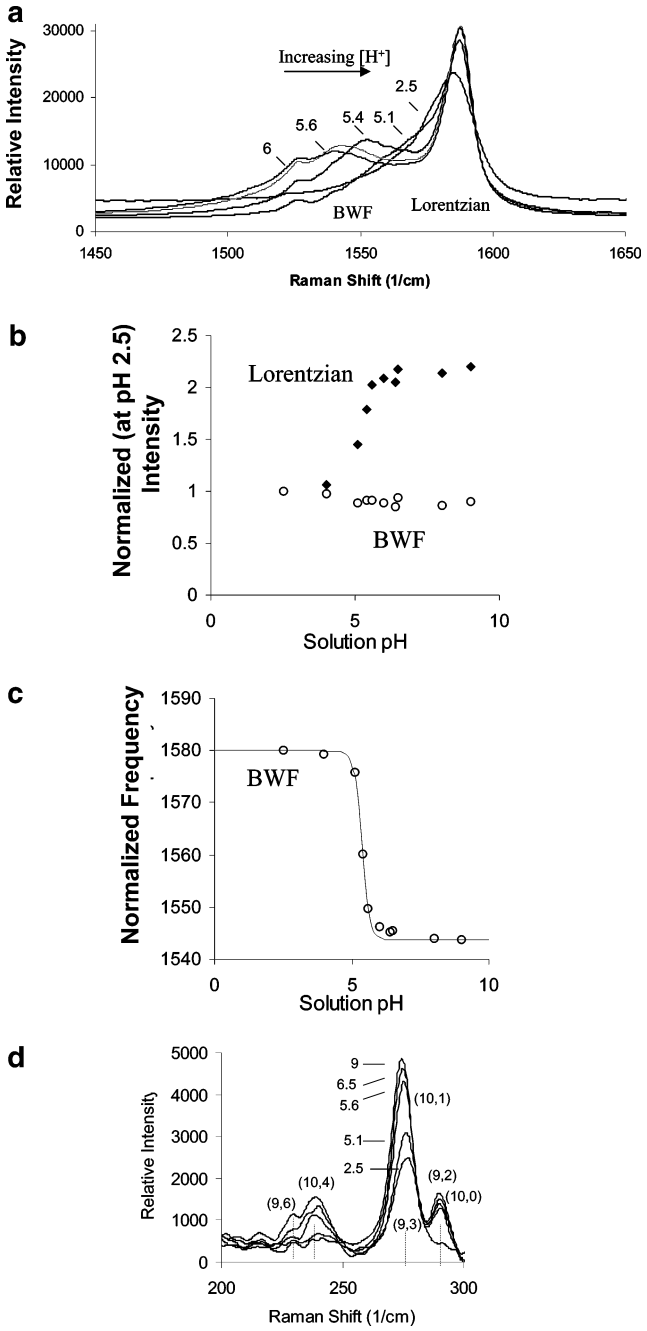

Figure 2. Raman spectra with excitation at 532 nm monitor the Fano line shape feature (peak I) of the tangential mode. It reflects phonon coupling to the electronic continua of metallic nanotubes. (a) This mode shifts to higher frequencies as the solution is acidified and restores as the pH is cycled back to alkaline. (b) Fitting this region of the spectrum to the Fano line shape (labeled BWF) and a Lorentzian for the remaining modes (labeled Lorentzian) demonstrates that only the latter decreases significantly in intensity. (c) The former shifts in a manner analogous to the absorbance in Figure 1. The smooth line is the model represented by eq 3. (d) At low Raman shift, the radial breathing modes of metallic semiconducting and one metallic feature are resonance-enhanced and show selective decay with increasing acidification.

the remaining Lorentzian (peak II), which falls by a factor of 2.2 with acidification. In this case, Raman scattering intensity is coupled to the absorption strength arising from singularities in the joint density of states near the excitation energy for a portion of the semiconducting nanotubes. Along with the characteristic peak shape, this lack of appreciable intensity decay of peak I in Figure 2b supports its interpretation as the BWF feature observed previously. However, the Raman frequency

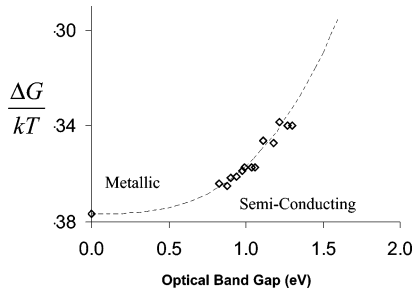

Figure 3. Values for the $\ln(K_p)$ as regressed using eq 2 for semiconducting nanotubes and eq 3 for metallic show a distinct trend with nanotube band gap. The smooth curve is a nonlinear free energy relation (eq 4) obtained empirically.

shift for this peak is 11 cm^{-1} higher than that observed by Kataura et al.,[13] who examined nanotubes synthesized with the same diameter range as those produced by the HiPco method (0.6−1.2 nm).[14] It should be noted that, unlike the samples prepared in this work, it is highly likely that metallic nanotubes in this case were in van der Waals contact with a random assortment of nanotube types. This is known to have a significant effect on the electronic structure of the tube, including the formation of a secondary gap[15] and shifting of the locations of energy levels relative to the case of the isolated tube.[5]

This uniform shifting with pH can be used as a measure of this phonon coupling; the shift to higher frequencies can be used to calculate an average reaction equilibrium constant for metallic nanotubes: Analogously, ω_p and ω_d are the peak-normalized

$$\frac{\omega(\mathrm{pH}) - \omega_p}{\omega_d - \omega_p} = 1 - \frac{K_p}{[H^+]^n + K_p} \qquad (3)$$

frequencies for the protonated and deprotonated state.

The Lorentzian feature at higher frequency shifts negligibly during the titration, unlike the case of other electron-transfer reactions.[10,16] This peak is comprised of contributions from predominately the semiconducting nanotubes, and shifts in this mode reflect force constant changes as the graphene plane stiffens with increasing electron withdrawal. Raman spectroscopy during pH cycling with excitation at 785 nm, which excites the E_{22} transitions of semiconductors for HiPco-produced nanotubes, also shows negligible shift. These observations can be used to place an upper limit on the number of electrons transferred per reaction. Kavan et al.[16] have determined that the tangential mode shifts 250 ± 80 cm^{-1} per electron per carbon atom when Raman spectroscopy is performed on an electrochemically tuned nanotube solution. Assuming that this trend is universal, a shift below the resolution of the Raman spectrometer (±1 cm^{-1}) as in these experiments sets as an upper limit of 16 electrons per 100 nm (10,10) nanotube. This upper bound supports the estimated value of three protons per chromophore during the reaction, as regressed from data in Figure 1a.

At lower Raman shift, two radial breathing modes corresponding to the semiconductors (9,2) and (10,0) are nearly resonant, with 532 nm excitation having second van Hove singularities at 551 and 539 nm, respectively. These features decay selectively with increasing acidification (Figure 2d). The metallic peaks (10,4), (10,1), and (9,6) are also resonant and respond to the lower pH before the semiconductors as predicted.

The equilibrium selectivity of the reaction appears to be well-correlated using the optical band gap as a reaction index. Figure 3 plots the normalized free energy change of reaction, $\Delta G/kT$, versus the band gap of the nanotube taken experimentally as

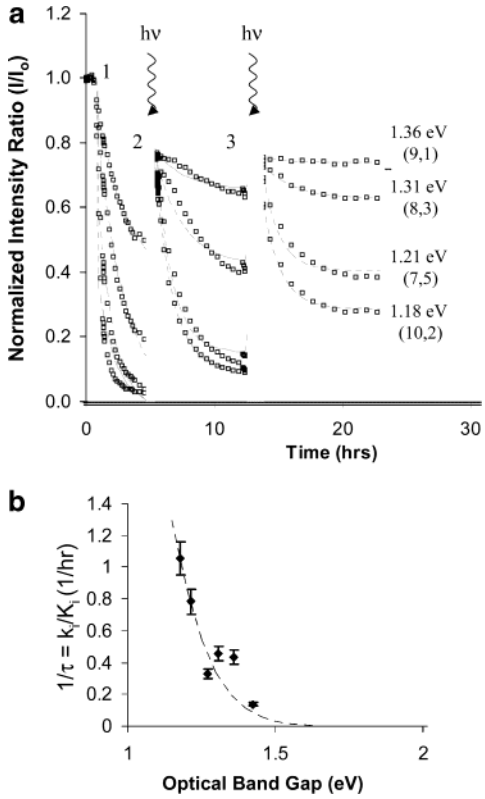

Figure 4. Photodesorption of O_2. (a) Spectral restoration, as monitored by tracking the fluorescence intensity of four small-diameter nanotubes, after acidifying the solution from pH 5.1 to 3.5 at point 1 under flowing N_2. At points 2 and 3, the solution was irradiated with a 4 min UV pulse from a low-pressure Hg lamp. The partial decay following each irradiation is first order and constant for a particular nanotube at all points. (b) These decay constants as a function of band gap can be scaled by the same dependence suggested by eq 4 and indicates a parity between equilibrium and kinetic selectivity for reaction at the nanotube sidewall.

the energy of its fluorescent emission (and zero for the metallic nanotubes). The trend suggests a nonlinear free energy relation for the reaction of the form:

$$\ln(K_p) = -\frac{\Delta G}{kT} = -\frac{\Delta G_m + \gamma(E_{gap})^{\beta}}{kT} \qquad (4)$$

Here, ΔG_m is the free energy change upon protonation of metallic nanotubes equal to 37.7 kT and γ and β are empirical fitted constants, 2 kT and 3, respectively. The latter reflect the stability of the homologous series of nanotubes to electron withdraw with increasing separation between the highest energy valence electrons and the Fermi level. The relation implies that H^+ forms a charge transfer complex at the sidewall, where the stability is directly related to the energy necessary to transfer charge to the adsorbate.

Oxygen Sensitivity. This pH sensitivity is only observed when samples have been exposed to O_2. This is illustrated by the observation that absorption intensity can be restored under acidic conditions by exposure of the solution to UV photons from a low-pressure mercury lamp while under a shelter gas. Reintroducing O_2 to the system at this point restores the original pH sensitivity and the absorption decreases. Figure 4a presents the normalized fluorescence intensities for four semiconducting nanotubes initially at pH 5.1 after heating the solution for 12 h at 40 °C under N_2. At this particular pH, these smaller diameter nanotubes are unreacted (see Figure 1a). After addition of HCl, acidifying the solution to pH 3.5, the fluorescence intensities fall to nearly zero over a period of 5 h. This equilibration time (>5 h) is notably longer than the times observed for an O_2-saturated sample and reflects the heating pretreatment of the sample in N_2 driving off some O_2.

At this state, a short (4 min) UV pulse partially restores the fluorescence as O_2 desorbs from the surface. After each pulse, the system relaxes to a new equilibrium state that is higher than the corresponding state before irradiation, and the extent of partial restoration appears to be electronically selective. Irradiation appears to decompose the reacting complex at the surface [P] and to remove O_2 as an adsorbate critical to its formation. Species desorbed from the surface but not the surfactant layer likely account for the transient following each pulse as they readsorb. It is also clear that the rate of reaction shows the same selectivity as a function of nanotube band gap or diameter as the equilibrium titration. The relaxation after irradiation shows characteristic first-order behavior and when normalized on the same absolute scale can be plotted to extract time constants for first-order decay ($1/\tau$) with $I = I_o \exp[-t/\tau]$. A single value of this constant can describe the response of a particular nanotube throughout the experiment. When plotted as a function of band gap, these constants show a similar nonlinear scaling as in the case of ΔG/kT (eq 4).

This irradiation process can be continued until full restoration is reached with the bulk solution remaining at pH 3.5, and the solution is stable to further acidification below pH 2. Changing the purge gas from 1 atm N_2 to O_2 then results in rapid reaction of the sample, as shown in Figure 5a for those nanotubes monitored by their enhanced radial breathing modes at 785 nm excitation and in Figure 5b using the fluorescence of some smaller diameter nanotubes during the same experiment. The effect of oxygen on nanotube electronic structure and reactivity is not fully understood. Chen et al.[17] demonstrate systematic conductance changes as their substrate mounted and semiconducting nanotube was exposed to O_2 and cleaned with UV irradiation. These authors claim that the O_2 withdraws electron density from the nanotube, creating a doped, p-type semiconductor of greater conductance. It is in fact remarkable that the transient profiles in this case resemble those in Figure 4a. However, Derycke and co-workers[18] claim that the interaction of O_2 in this case predominately changes transport barriers at the nanotube−metal contact, causing the observed change. Martel and researchers[19] grafted nanotubes to a TiC substrate and showed that annealing at 800 °C along with sealing in a SiO_2 layer creates an ambipolar device that is stable in air. While there is no analogue of a semiconductor−metal junction in the solution phase, it is unlikely that O_2 itself is withdrawing electron density, as its adsorption is undetectable using the spectroscopic methods developed in this work. It is more likely that O_2 catalyzes the interaction of H^+ with the nanotube sidewall by either lowering the energetic barrier for reaction or participating in the complex directly.

Many studies have attempted to model O_2 adsorption on nanotube surfaces and its effect on electronic structure. Jhi and Cohen[20] state that oxygen binds strongly to the surface of carbon nanotubes with a predicted bond energy of 0.25 eV for an (8,0) nanotube and withdraws approximately 0.1 electron per adsorbed molecule. Here, the O_2 interacts strongly with lower lying electronic orbitals and has little effect on the highest energy valance band. Ricca and co-workers[21] used the ONION method with MP2 correlation for long-range interactions. The authors found that O_2 chemisorption is unfavorable at room temperature, and physisorption is weak but stable at 2.67 kcal/mol. Very little charge transfer is anticipated from the latter calculations. In this

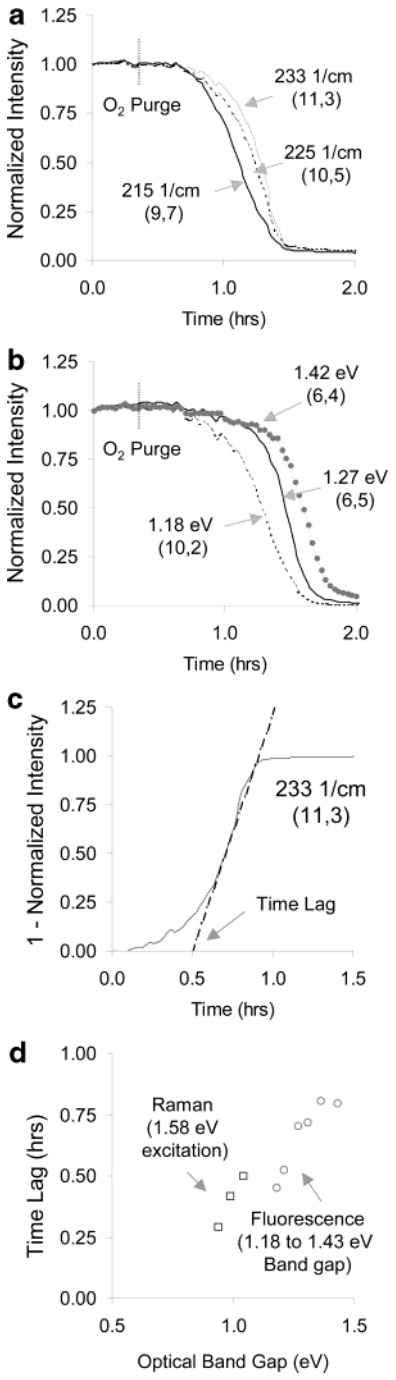

Figure 5. A solution of suspended nanotubes at pH 2 purged of 1 atm O_2 by UV irradiation fluoresces at maximum intensity and Raman radial breathing modes at 785 nm excitation show maximal enhancement while under an N_2 purge. At the indicated time, the purge gas is switched to O_2 and enhanced Raman scatter diminishes (a) along with fluorescence (b). Here, the forward reaction (eq 5) is large as oxygen is reintroduced and the system becomes rapidly equilibrium-limited, hence the second-order behavior. (c) The second-order response can be characterized by the time lag—an extrapolation of the line at the inflection point to the time axis. (d) Selectivity upon O_2 addition as characterized by the time lag also shows a band gap dependence.

work, oxygen is apparently critical to enable the reaction, but by spectroscopic means (using either Raman scatter, absorption or fluorescence) its adsorption on the nanotube is undetectable. This tends to support the latter calculation of negligible charge transfer.

Regardless of the nature of the interaction, it is clear from the above observations that O_2 plays a critical role in the reaction. Its effect appears to be highly localized, since not only the equilibrium selectivity (as evidenced by the partial restoration) but also the rate of reaction is dependent upon UV exposure history and hence the O_2 surface coverage. With this in mind, one can model the rate of formation of the protonating complex [P] as

$$\frac{d[P]_i}{dt} = k_i[H^+][O_2]_i - \frac{k_i}{K_i}[P]_i \quad (5)$$

where k_i is a pseudo-first-order rate constant and $[P]_i$ is the surface concentration of protonating species on a particular nanotube. In the UV photodesorption experiments, eq 3 can be integrated to yield the normalized surface coverage of [P] as a function of time following a step change in surface oxygen coverage (as with desorption from a UV pulse):

$$\alpha(t) = \frac{[P](t)}{[P]_{Total}} = \frac{[O_2][H^+]K_i}{[P]_{Total}} + \exp\left(-\frac{k_i}{K_i}t\right)\left(\frac{[P]_o - [O_2][H^+]K_i}{[P]_{Total}}\right) \quad (6)$$

This ratio α, the fraction of protonated sites on the nanotube, is monitored directly using the normalized fluorescence intensity, which is related to the deprotonated state:

$$\frac{I_o - I(t)}{I_o} = \frac{[P](t)}{[P]_{Total}} = \alpha(t) \quad (7)$$

Equations 4 and 5 are used to fit the dynamic response of the system following a UV pulse, as shown by the dotted curves in Figure 4a. A single value of the rate constant, k_i, can be used to regress the entire response for each semiconductor after a series of irradiations. Figure 4b plots k_i/K_i versus the band gap of the nanotube. This ratio is the inverse time constant of the response and is constrained experimentally by the dynamics of the fluorescent emission after UV irradiation in this way. From Figure 4b, it is clear that the equilibrium selectivity observed in the titration above is also observed in the relative rates of reaction after photodesorption of oxygen.

By examining the percent restoration of each species after UV irradiation as a function of time, it is possible to estimate the O_2 photodesorption cross sections for each nanotube using an estimated photon flux from the UV lamp of 1.5×10^{16} photons/cm^2/min. Plotting the logarithm of the initial protonation rate following each exposure versus time yields a linear relationship with slope $\sigma_i F$ where F is the flux and σ_i is the desorption cross-section for species i. Values for the latter range from 1.5×10^{-17} cm^2 for the (10,2) nanotube to 3.5×10^{-17} cm^2/photon (9,1). The generally increasing trend with decreasing diameter is consistent with the premise of greater charge transfer from smaller band gap nanotubes strengthening this interaction and decreasing desorption probability. Chen and co-workers[17] estimate a cross section of 1.4×10^{-17} cm^2/photon for a large diameter nanotube ($E_{gap} \sim 0.6$ eV) from conductance increases following O_2 desorption, and this value is commensurate with those reported in this work.

Examining the selectivity observed upon reexposure to O_2 can further elucidate the role of oxygen. This is illustrated in Figure 5a,b, where oxygen is rapidly replaced under acidic conditions (pH 2) to a system that has been deoxygenated by UV exposure. Here, the rate is necessarily limited by the oxygen adsorption kinetics and the selectivity is shown again to vary

with band gap. Because an excess of O_2 is exposed to the solution, the reverse reaction in eq 3 is large and the system becomes equilibrium-limited. The process displays second-order behavior reflecting this limitation, and the time lag as measured by extrapolation of the rate at the inflection point to the time axis (Figure 5c) characterizes the selectivity of the reaction with O_2 as the limiting reagent. Plotted as a function of the band gap, monotonically increasing but distinct trends are demonstrated for both fluorescence and resonance-enhanced Raman scattering (Figure 5d). Here, we observe that the fluorescence intensity is diminished earlier, reflecting its greater sensitivity to the localization of the highest lying valence electrons. Using the diminishment of resonance enhancement as the measure, the curve is apparently shifted to longer times as a greater extent of reaction is needed to affect the absorption and resonant Raman scatter. This can be understood as the exciton[22] being formed upon absorption as a local event on the nanotube sidewall and, unlike the subsequently formed excited state, is relatively insensitive to reactive centers far from the site of formation.

The Role of the Surfactant Layer. The electronic double layer produced at the water/surfactant interface around the nanotube influences the local hydronium ion concentration in solution. Because of this, the pH sensitivity described above is strongly influenced by the chemical nature of the surfactant employed. In general, for an ionic suspending agent, the ionic moieties of the adsorbed surfactant layer can act as sites for ion exchange via

$$[H^+] + [S] \overset{K_e}{\leftrightarrow} [H^+]_m \quad \text{where} \quad [S] = C_T - \text{cmc} \qquad (8)$$

Consequently, species that compete favorably for the exchange sites [S] decrease the interfacial hydronium ion concentration $[H^+]_m$. For example, PVP demonstrates strong complexation to SDS in solution via charge transfer from the sulfate groups, and hence, this polymer is believed to adsorb strongly to the external surface of the adsorbed SDS layer (SDS−PVP). This adsorption is a competitive exchange of available sulfate groups, substantially lowering the interfacial pH as in the case of ketal acid hydrolysis in surfactant solution.[23]

Suspended carbon nanotubes show a partial restoration of the fluorescence and absorption spectrum after complete protonation at pH 2 upon addition of 0.1% PVP. This restoration is in fact general for all such complexing polymers and species. To account for the role of the surfactant, we apply eq 8 to eq 2 with the goal of calculating the intrinsic nanotube protonation constants:

$$\frac{A(\text{pH}) - A_p}{A_d - A_p} = \frac{K_p}{[H^+]_m + K_p} = \frac{K_p}{\dfrac{[H^+]K_e}{[S]} + K_p} = \frac{K_p}{10^{(\text{pH}+\Delta\text{pH})} + K_p} \qquad (9)$$

Here, the surfactant effectively shifts the spectroscopic response of the system to more neutral conditions by changing the interfacial pH by an amount ΔpH.

Values for the shift in protonation equilibrium of semiconducting nanotubes used in this work are listed in Table 1 with ΔpH values compared to literature findings for SDS and SDS/PVP mixtures. Using nanotubes as the pH sensitive chromophore, PVP and PEO produce similar ΔpH values. These polymers have saturated the micellar surface and show no additional shift with increasing molecular weight above 40 kDa or concentration greater than 0.1 wt %. This interpretation is supported by the behavior of 1-vinyl-2-pyrrolidone, the monomer of PVP, which demonstrates an increasing shift in pH with increasing concentration and saturation only with full restoration. Long-chain alcohols also display this behavior but do not occupy [S] sites, rather their incorporation into the adsorbed layer displaces a sulfate group, with the OH orientated into solution. This increases the packing density of the adsorbed layer as charge repulsion at the headgroups is reduced, but it still results in the loss of exchange sites as SDS is displaced. Of ultimate importance is the observation that sodium dodecyl sulfate obscures the true protonation equilibrium, shifting the behavior to more neutral pH in a predictable manner. From Table 1 it is evident that the intrinsic proton behavior of the semiconducting nanotubes in Figure 1a is such that the reaction takes place approximately between pH 4 and pH 1, when corrected for the increase in $[H^+]$ at the surfactant/water boundary.

TABLE 1: Comparison of Protonation in Various Surfactant Media

system	concn (wt %)	ΔpH	K_e/[S]	ΔpH from SDS
sodium dodecyl sulfate (SDS)[a]	1	2	1	0
poly(vinylpyrrolidone 40 kDa/1% SDS[a]	1	0.2	63	1.8
poly(ethylene oxide) 70 kDa/1% SDS[b]	0.1	−0.1	0.79	2.1
poly(ethylene oxide) 70 kDa/1% SDS[b]	1	−0.1	0.79	2.1
poly(vinylpyrrolidone 40 kDa/1% SDS[b]	0.1	−0.15	0.71	2.15
poly(vinylpyrrolidone 40 kDa/1% SDS[b]	1	−0.15	0.71	2.15
poly(vinylpyrrolidone 360 kDa/1% SDS[b]	0.1	0.4	2.51	1.6
1-vinyl-2-pyrrolidone/1%SDS[b]	0.67	−0.4	0.40	2.4
1-vinyl-2-pyrrolidone/1%SDS[b]	1.33	−1	0.10	3
1-vinyl-2-pyrrolidone/1%SDS[b]	2	−1.3	0.05	3.3
dodecyl trimethylammonium bromide[b]	1	<-4		

[a] Using a pyridine-2-azo-*p*-dimethylaniline chromophore.[23] [b] This work, using the titration curves in Figure 1b for the 0.98 eV (8,7) and 1.12 eV (7,5) band gap semiconducting nanotubes in SDS as reference.

Conclusions

Acidification of a solution of surfactant-dispersed single-walled carbon nanotubes in water results in a reaction with H^+ at the sidewall that localizes valence electrons. The reaction can be monitored as a loss of absorption intensity for transitions corresponding to the 1st van Hove singularity, a reduction in resonance enhanced Raman scatter, and quenching of fluorescent emission from the nanotube. The process is completely reversible as solution pH is cycled from acidic to basic conditions and equilibrium constants are shown to vary significantly with nanotube band gap. Metallic nanotubes appear most sensitive to pH with $\ln(K_p)$ equal to −37.7 and the smallest diameter semiconducting nanotubes (largest band gap) least reactive with a value of −34. Adsorbed O_2 from solution is shown to play a critical role, controlling both the rate and the equilibrium extent of reaction. Using the surface reaction as a probe of the surfactant/water interface, we show that the nature of the surfactant shifts the pH behavior to higher or lower values systematically in a manner consistent with a pseudo-phase ion exchange model. The reaction, which demonstrates chemical specificity toward nanotube electronic structure, is the first such systematically reversible reaction pathway identified for nanotubes in solution. The result holds promise for chemically selective functionalization as well as separation and selection of nanotubes of certain electronic and physical properties.

Acknowledgment. Financial support was provided by the NSF Focused Research Group on Fullerene Nanotube Chemistry (DMR-0073046), the NSF Center for Biological and Environmental Nanotechnology (EEC-0118007), and the Robert A. Welch Foundation (C-0689). Support from NASA (NCC9-77) for development of the HiPco method is also gratefully acknowledged.

Note Added after ASAP Posting. This article was posted ASAP on 6/25/2003. The reaction in eq 1 has been modified. The correct version was posted on 6/26/2003.

References and Notes

(1) Dresselhaus, M. S.; Dresselhaus, G.; Eklund, P. C. *Science of Fullerenes and Carbon Nanotubes*; Academic Press: San Diego, 1996.

(2) Saito, R.; Dresselhaus, G.; Dresselhaus, M. S. *Physical Properties of Carbon Nanotubes*; Imperial College Press: London, 1998.

(3) Girifalco, L. A.; Hodak, M.; Lee, R. S. *Phys. Rev. B* **2000**, *62*, 13104−13110.

(4) Thess, A.; Lee, R.; Nikolaev, P.; Dai, H. J.; Petit, P.; Robert, J.; Xu, C. H.; Lee, Y. H.; Kim, S. G.; Rinzler, A. G.; Colbert, D. T.; Scuseria, G. E.; Tomanek, D.; Fischer, J. E.; Smalley, R. E. *Science* **1996**, *273*, 483−487.

(5) Reich, S.; Thomsen, C.; Ordejon, P. *Phys. Rev. B* **2002**, *65*, 155411.

(6) Bahr, J. L., Tour, J. M. *J. Mater. Chem.* **2002**, *12*, 1952−1958.

(7) Chen, J.; Hamon, M. A.; Hu, H.; Chen, Y. S.; Rao, A. M.; Eklund, P. C.; Haddon, R. C. *Science* **1998**, *282*, 95−98.

(8) O'Connell, M. J.; Bachilo, S. M.; Huffman, C. B.; Moore, V. C.; Strano, M. S.; Haroz, E. H.; Rialon, K. L.; Boul, P. J.; Noon, W. H.; Kittrell, C.; Ma, J.; Hauge, R. H.; Weisman, R. B.; Smalley, R. E. *Science* **2002**, *297*, 593−596.

(9) Yu, Z. H.; Brus, L. E. *J. Phys. Chem. A.* **2000**, *104*, 10995−10999.

(10) Chiang, I. W.; Peng, H.; Stevenson, J.; Smalley, R.; Margrave, J. L.; Hauge, R. H. *J. Phys. Chem. B.* Submitted.

(11) Bachilo, S. M.; Strano, M. S.; Kittrell, C.; Hauge, R. H.; Smalley, R. E.; Weisman, R. B. *Science* Submitted.

(12) Brown, S. D. M., A. Jorio, and P. Corio, M. S. Dresselhaus, G. Dresselhaus, R. Saito, K. Kneipp. *Phys. Rev. B* **2001**, *63*.

(13) Kataura, H.; Kumazawa, Y.; Maniwa, Y.; Umezu, I.; Suzuki, S.; Ohtsuka, Y.; Achiba, Y. *Synth. Met.* **1999**, *103*, 2555−2558.

(14) Zhou, W.; Ooi, Y. H.; Russo, R.; Papanek, P.; Luzzi, D. E.; Fischer, J. E.; Bronikowski, M. J.; Willis, P. A.; Smalley, R. E. *Chem. Phys. Lett.* **2001**, *350*, 6−14.

(15) Itkis, M. E.; Niyogi, S.; Meng, M. E.; Hamon, M. E.; Hu, H.; Haddon, R. C. *Nano Lett.* **2001**, *2*, 155−159.

(16) Kavan, L.; Rapta, P.; Dunsch, L.; Bronikowski, M. J.; Willis, P.; Smalley, R. E. *J. Phys. Chem. B.* **2001**.

(17) Chen, R. J.; Franklin, N. R.; Kong, J.; Cao, J.; Tombler, T. W.; Zhang, Y.; Dai, H. *Appl. Phys. Lett.* **2001**, *79*, 2258.

(18) Derycke, V.; Martel, R.; Appenzeller, J.; Avouris, P. *Appl. Phys. Lett.* **2002**, *80*, 2773−2775.

(19) Martel, R.; Derycke, V.; Lavoie, C.; Appenzeller, J.; Chan, K.; Tersoff, J.; Avoruris, P. *Phys. Rev. Lett.* **2002**, *87*.

(20) Jhi, S., Louie, S. G., Cohen, M. L. *Phys. Rev. Lett.* **2000**, *85*, 1710−1713.

(21) Ricca, A.; Drocco, J. A. *Chem. Phys. Lett.* **2002**, *362*, 217−223.

(22) Ando, T. *J. Phys. Soc. Jpn.* **1997**, *66*, 1066−1073.

(23) Zanette, D., Froehner S. J., Edson Minatti, E., Ruzza, A., A. *Langmuir* **1997**, *13*, 659−665.